ORIGINAL RESEARCH

Fused filament fabrication printing process of polymers highly filled with metallic powder: a significant influence of the nozzle radiation on the substrate temperature

A. Thézé[1,2] · G. Régnier[1] · A. Guinault[1] · S. Richard[2] · B. Macquaire[2]

Abstract

Extending fused filament fabrication process to feedstock materials used in metal injection molding could be a solution to produce the so-called green part. Nevertheless, process conditions could lead to low mechanical properties partly due to a lack of adhesion between the filament and the substrate. Thus, it is important to estimate correctly the temperature at the substrate interface induced by the filament deposition. Knowing that the extrusion printhead is a relative massive steel part moving at a small distance of the substrate, we have determined the radiative effect of nozzle passages on the temperature surface of the substrate. For that, we inserted thermocouples having a diameter of 0.25 mm under the substrate surface at a depth of 0.45 mm. Thermocouples measured an increase of temperature between 1.1 and 1.4 °C depending on the controlled nozzle and substrate temperatures. A 2D finite-difference model allows determining a significant increase of the substrate temperature at the surface varying between 3.5 and 5 °C depending on processing conditions. This increase of interface temperature, which is favorable to the adhesion of the filament to another one, can be advantageously considered.

Keywords Fused Filament Fabrication · Fused Deposition Modeling · Feedstock · Reinforced polymers · Nozzle radiation

Introduction

Metal injection molding (MIM) is a process in which fine metal powder is mixed with a polymeric binder material to create a "feedstock" material. Then this feedstock is shaped using injection molding process in the same way than for thermoplastics molding [1]. This molding process allows large series and complex geometry parts. After molding, the fragile part called "green part" undergoes conditioning operations to first remove the binder (debinding process) at intermediate temperatures and then to sinter the powder at high temperatures close to the metal fusion temperature to achieve part densification. Finished parts are generally small metallic components used in many industries and applications.

Due to high costs of tools and lead time, additive manufacturing of green parts through fused filament fabrication process (FFF) process is developing a lot for prototyping or small series [2, 3]. To obtain the metallic part, the green parts manufactured by FFF process follow the same debinding and sintering steps than for MIM process.

In FFF process, the extruded filament is deposited on the previous solidified layer and should bond to this substrate to ensure a good material cohesion. This cohesion between filaments is a key problem for FFF process to obtain good material properties and should be optimized. This adhesion is governed by two keys phenomena: intimate contact between filaments and then interdiffusion of polymers chains across the interface [4]. Intimate contact modelling is often based on a fine description of the surface roughness and a squeezing flow if a pressure can be applied, which is not really the case for FFF process. The only possible applied pressure is induced by the squeezing of the melted filament on the substrate. Then wetting or dewetting effects should play a role [5]. The interdiffusion of polymer chains can be modelled by chain motion reptation theory introduced by De Gennes [6]

✉ G. Régnier
gilles.regnier@ensam.eu

1. PIMM Laboratory, Arts et Métiers Institute of Technology, CNAM, CNRS, Hésam Université, 151 bd de l'Hôpital, 75013 Paris, France

2. Safran Tech, Materials and Processes, Rue de Jeunes Bois, Chateaufort, 78114 Magny-Les-Hameaux, France

and Doi and Edwards [7]. In anisothermal processes, Yang and Pitchumani [8] shown that the interdiffusion of polymer chains can practically be modelled by a criterium based on rheological measurements. As these two phenomena are highly enhanced by temperature and time, it is valuable to increase the nozzle temperature, but the upper bound defined by material suppliers to avoid the organic matrix degradation is quickly reached. If the increase of nozzle temperature is not sufficient to ensure a good adhesion for some materials, some FFF machines propose a controlled heated build plate and still most sophisticated FFF machines a whole work area inserted in a controlled heated chamber.

Additional heating systems can be mounted around the nozzle to increase the subsequent layer or the substrate temperature. Partain [9] used a hot forced air system around the extrusion nozzle to increase the underlying material temperature, Striemann et al. [10] used an infrared preheating system, while Ravi et al. [11] and [12] used a laser to increase interface temperature.

Another difficult challenge is to estimate the increase of temperature at the substrate surface. Seppala et al. [13] and Lepoivre et al. [14] used infrared thermography, but they mainly monitored the cooling of the deposited material. The interface temperature was directly measured by putting thermocouples along the nozzle trajectory, but Xu et al. [15] mentioned in their paper how controlling the precise location of the thermocouples is a fastidious task. Deshpande et al. [12] put thermocouples on the molten substrate to soften it. Then, a pressure was applied on the surface to drown thermocouples at the feedstock surface thanks to a laboratory press and a specific aluminum tool. But the size of the thermocouple head does not allow precisely defining the interface location. To assess the interface temperature, the use of a thermal modelling fit on some thermal measurements seems to be a good way [15].

However, the metallic extrusion head, which moves at a small distance of the substrate can also modify the evolution of interface temperature by thermal radiative effects. This heating generated by the simple passage of the extrusion nozzle has not been extensively studied. Wolszczak et al. [16] studied the temperature distribution of deposited material using IR camera. They assessed an increase of subsequent layer temperature by the heat emitted by the head. Although this heating is not directly identified, the authors hypothesized that the geometry of the head and the printing conditions could increase this effect. Cosson et al. [17] also studied the nozzle preheating by means of an IR camera. Then they developed a 2D thermal model to quantify the heating effects of the nozzle radiation by comparing the cooling rates of the deposited filaments with and without nozzle radiation. According to their results, a significant effect was predicted on the cooling rate of deposited filaments, especially when the printhead speed is low. Thus,

neglecting heat emitted by nozzle would lead to overestimated cooling rates and then a potential higher crystallinity of the feedstock matrix, which could modify its mechanical properties. Bedoui and Fayolle [18] demonstrated the direct link between crystallinity rate and mechanical properties on polyoxymethylene, which often enters in feedstock composition.

This paper aims to analyze and quantify the radiative effect of nozzle passage over the substrate in FFF process by instrumenting the substrate with thermocouples inserted at 0.45 mm under the surface to not disturb the thermal field at interface and to quantify the evolution of the interface temperature with a simple 2D thermal model.

Experimental

Material properties

The feedstock studied in this paper is a 17-4 PH stainless steel powder mixed with a polymer matrix, which plays the role of binder. This green material contents 64% in volume of metallic powder and has a density of 5.54 g/cm^3. The matrix binder is mainly composed of polyoxymethylene (POM) in which is added a small amount of polypropylene (PP). The PP trace can be seen in cooling at about 110 °C on the thermogram measured on a TA Instrument Q10 DSC at 30 °C/min (Fig. 1). This DSC thermogram in heating and cooling highlights a melting temperature peak around
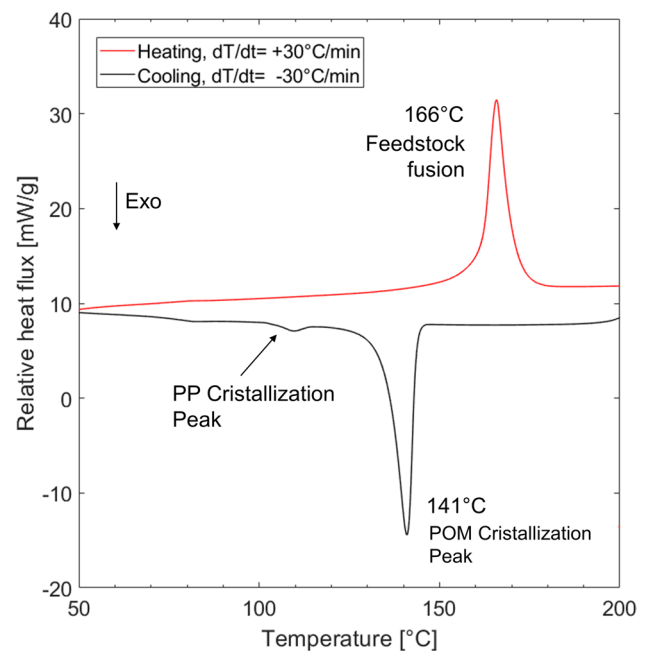
Fig. 1 DSC Thermogram of the feedstock in heating and cooling at 30 °C/min

166 °C and a crystallization which occurs around 141 °C at 30 °C/min, these peaks are the ones of POM.

The thermal conductivity was measured using the line source method according to ASTM D5930 09 from a K-system II of Advanced CAE technology Inc. at atmospheric pressure in cooling mode. A value of 1.89 W/(m.K) was found between 100 and 150 °C, close to the theoretical value of 1.85 W/(m.K) determined by a Maxwell homogenization model [19].

The specific heat was measured on a calorimeter (DCS1 Mettler Toledo) according to ISO 11357 in heating and cooling mode at 10 °C/min. As the feedstock is not melted in this study, with a temperature varying between 90 and 140 °C, its specific heat is considered as constant in that temperature range being 660 J/(kg.K).

Fused filament fabrication machine and processing conditions

A high temperature FFF machine manufactured by Intamsys® was used. The extrusion head moves in the xy plane over the metallic build plate moving along z axis. All nozzle displacements were computed by G-codes and uploaded with Simplify3D® software. Some technical modifications were also made on the extrusion head to process the 1.75 mm diameter feedstock filament.

In this paper, the distance between extrusion nozzle and the feedstock substrates was chosen at 0.2 mm and 0.4 mm. A steel nozzle with a diameter of 0.6 mm was used. The nozzle temperature varied in the tests between 190 and 220 °C. The feedstock substrates were fixed on the machine build plate, which temperature was regulated between 80 and 130 °C. These ranges of temperature were chosen knowing that using a nozzle at 190 °C and a substrate below 100 °C did not allow the deposited material to be properly welded on the previous layer.

The machine has a controlled heated build chamber to keep thermal conditions stable until 90 °C, thanks to a forced air convection system. All these temperatures were monitored through several K-type thermocouples connected to a multiplex temperature recorder. In the whole study, the printhead speed was set at a constant value of 20 mm/s.

Measurement of temperature history

As it is not easy to directly measure the interface temperature by IR measurements, we chose to determine this temperature evolution by a thermal simulation fitted on thermal measurements performed by thermocouples precisely located at 0.45 mm from the substrate surface to not disturb the thermal field at the substrate surface. As the response time of thermocouples is linked to the diameter of the probe, using the smallest thermocouples available was a priority.

However, drilling holes smaller than 0.3 mm in the feedstock without losing precision on holes positioning was not possible because the poor evacuation of chips leads to the break of the drilling tool. Then, holes with a diameter of 0.3 mm were precisely drilled with a CNC machine at 0.45 mm depth from the surface of an injection molded feedstock plate ($2.5 \times 13.5 \times 92$ mm3) (Fig. 2). Then, the temperature history was recorded at a frequency of 1 kHz by a multiplex temperature recorder connected to K-type thermocouples inserted in a sheath of 0.25 mm in diameter supplied by Tc Direct.

Thermocouples were calibrated using fixed point method [20]. This method consists of using phase change temperature of a substance to control thermocouples measurements. The typical signals recorded from the thermocouples when they were dipped from room temperature into boiling water are shown on Fig. 3. The time constant of a thermocouple defined as the time required to respond to 63.2% of an instantaneous temperature change was measured at 0.014 s in boiling water, so the full temperature detection is reached after about 0.04 s, three times the time constant.

The thermocouples were inserted in the 0.3 mm diameter holes with a thermal compound to ensure a good thermal contact. Another thermocouple was located a few millimeters above the deposition surface and far away from the extrusion nozzle to record the build chamber temperature. Figure 4 gives an example of temperature history recorded at depth of 0.45 mm below the surface of the substrate during the passage of the nozzle at 220 °C without extruding any filament. A rise of the temperature just after the passage of the extrusion nozzle over the substrate can be clearly observed.
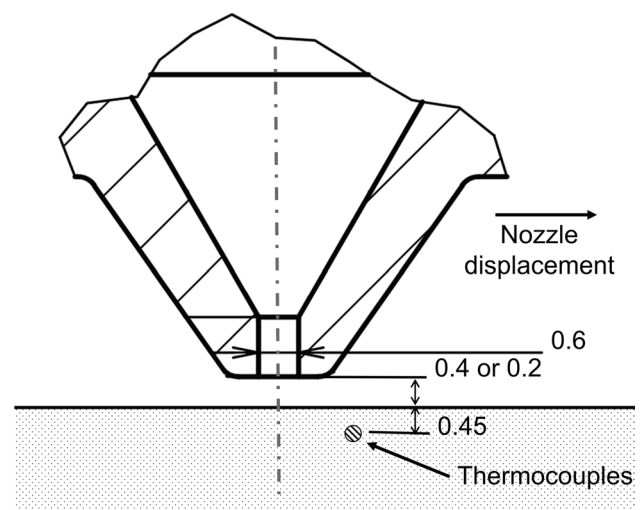
Fig. 2 Schematics of substrate instrumentation and extrusion nozzle (dimensions in mm)
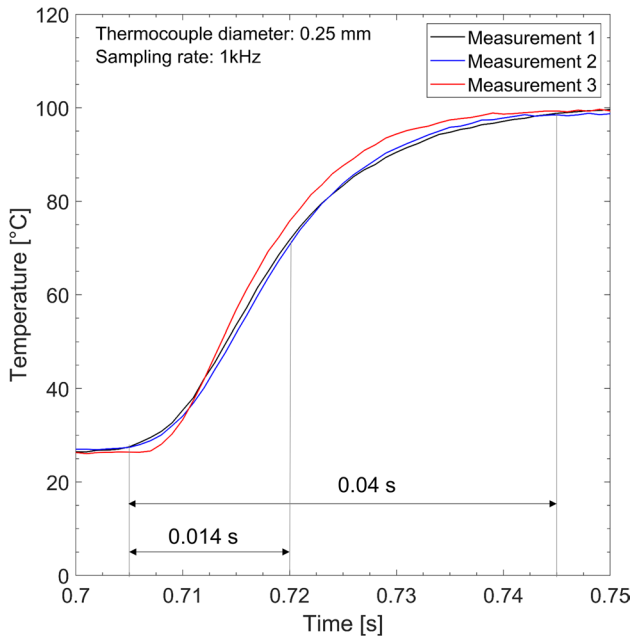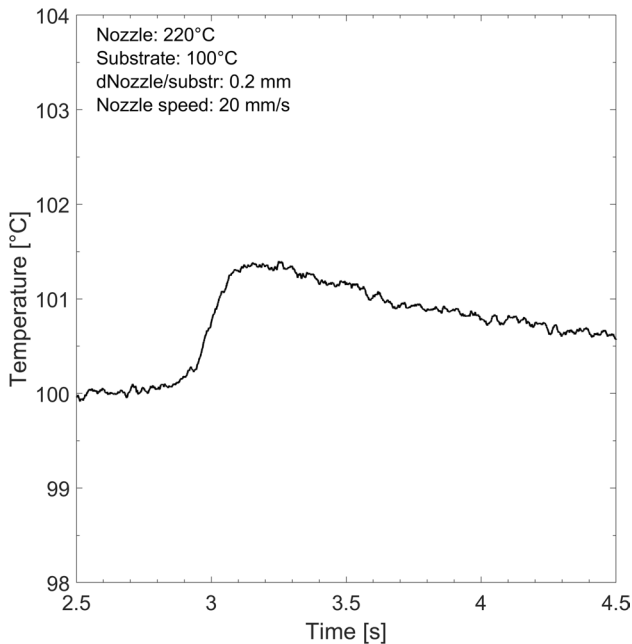
Fig. 3 Response time measurement of thermocouples dipped in boiling water

Thermal modelling

General formulation

A simple numerical model using finite-difference method

Fig. 4 Evolution of temperature at 0.45 mm depth in the substrate during a nozzle passage at 0.4 mm from the substrate

with an explicit scheme was built on Matlab® code to predict the temperature in the substrate. Knowing that the nozzle is wide enough compared to heat time penetration to reach the thermocouple, it was decided to use a 2D modelling instead of a 3D one to reduce time calculation. The principle of modelling and the phenomena considered are shown schematically in Fig. 5.

As described in Fig. 5, the chosen boundary conditions on the upper surface of the feedstock substrate are convection condition with the heated air of the build chamber and adiabatic condition on lateral sides of the modelled substrate. Thermal exchanges inside the substrate are only conduction. The heat transfer from the hot nozzle is considerate as a source term moving along first layer elements.

The substrate is 5 mm long in the modelling, this dimension is considered sufficiently large compared the observed thermal domain between the thermocouple and the surface of the substrate. We ensured that the boundary conditions on this limited modelled domain did not impact the thermal results. The lower part of the substrate is set on the heated and regulated build plate. A contact resistance between the substrate and the regulated build plate was set.

Conduction

The substrate was considered as a homogenous material with a constant thermal conductivity λ and a constant specific heat C_p. Inside the substrate, only conduction occurred and the thermal balance on a volume element (Fig. 6) can be simply written as:

$$V \rho \, C_p \frac{dT}{dt} = S_l(q_w + q_e) + S(q_n + q_s) \qquad (1)$$

where V is the volume of the element, S_l the lateral surfaces of the element, S the upper or lower surface of the element and q_i the thermal flux on these surfaces. Then, the temperature $T_{n+1,i,j}$ of a volume element at time $n+1$ and at the location i,j can be easily determined in an explicit scheme from Eq. (1) by the following discretized formulation:

$$l_x l_y \rho \, C_p (T_{n+1,i,j} - T_{n,i,j})$$
$$= \Delta t \lambda \left[l_y \left(\frac{T_{n,i-1,j} + T_{n,i+1,j} - 2T_{n,i,j}}{l_x} \right) + l_x \left(\frac{T_{n,i,j-1} + T_{n,i,j+1} - 2T_{n,i,j}}{l_y} \right) \right] \qquad (2)$$
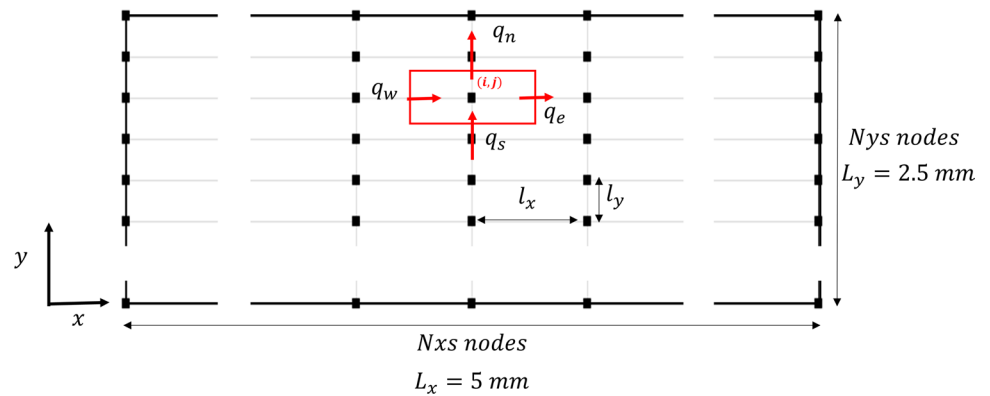
Convection

The volume elements located at the top of the substrate have conduction exchanges with adjacent elements and potential heat exchanges by convection with the air of chamber. The additional convection flux $\Phi_{convection}$ can be defined as:

Fig. 5 Thermal exchanges modeling
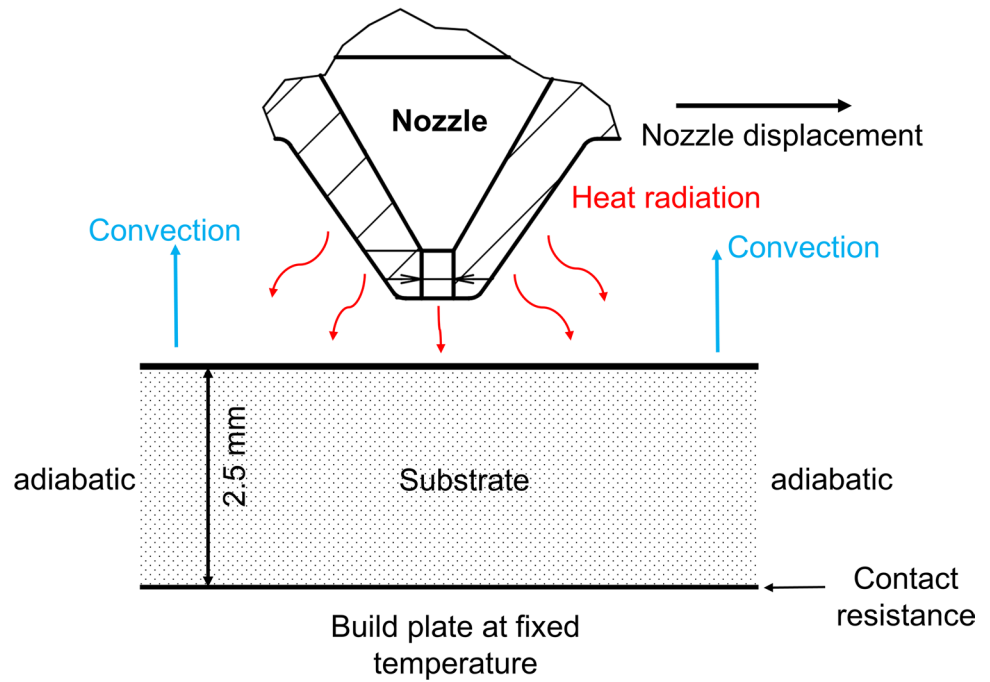

Fig. 6 2D Mesh and dimensions used in the model

$$\Phi_{convection} = h \, S(T_{substrate} - T_{air}) \qquad (3)$$

where h is the heat exchange coefficient. Several values of heat exchange coefficient are used in literature. Between ABS and air, Rodriguez et al. [21] used a heat exchange coefficient equal to 62 W/(m² K) and Xu et al. [15] used a heat exchange between 13 and 8 W/(m² K). Lepoivre et al. [14] used a heat exchange coefficient equal to 30 W/(m² K) to simulate cooling of ABS and PEKK. Bellehumeur et al. [22] studied the influence of the heat exchange coefficient for ABS and found a value of about 30 W/(m² K) for a build chamber regulated at 70 °C.

A value of 30 W/(m² K) has a low influence but not insignificant on the temperature evolution during the few seconds of the simulated experiment. Then, as we waited typically 15 min before any experiments to ensure thermal equilibrium, we could consider than the heating of the build plate compensated the lost thermal flux exchanged by convection without creating a significant thermal gradient in the substrate, which is quite conductive with its high content of metallic powder particles. No significant thermal gradients were observed between thermocouple measurements in the substrate at 0.45 mm and 0.75 mm in stabilized regime. Therefore, all simulations were conducted without convection and without thermal heating input in the build plate.

The non-perfect contact between the substrate and the regulated build plate was treated as a convective flux by adding a contact resistance equal to the inverse of a heat exchange coefficient. The thermal contact resistance was set to 2×10^{-4} m² K/W to fit the cooling of the substrate measured by the thermocouples. This value is consistent with the value determined between a polymer in contact with a metallic injection mold [23].
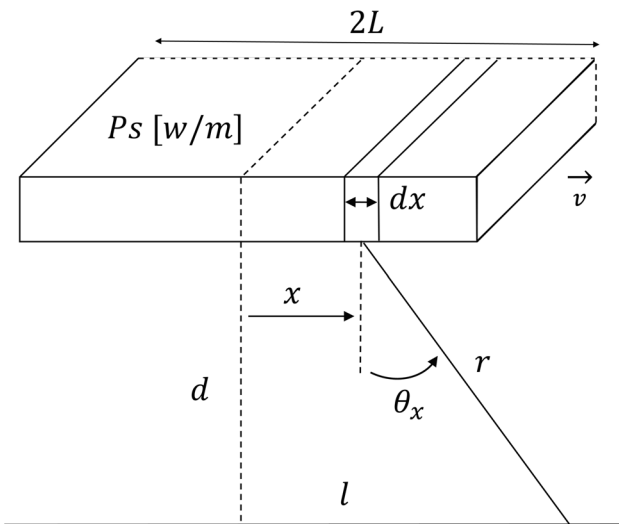
Fig. 7 Schematics of radiation source modelling

Fig. 8 Influence of extrusion head on the increase of local substrate temperature

Nozzle radiation modeling

To take in account the radiation of nozzle, a heat source passing over substrate was added in the model. The print-head was considered as a 2D heat source having a length of 3 mm and moving over the substrate at a height d with a velocity v (Fig. 7). We considered that all the emitted radiation is absorbed by the feedstock substrate.

The elementary flux density dq emitted by an elementary width dx of the 2D heat source and absorbed by the substrate at a distance l from the center of the 2D power source is:

$$dq = \frac{P_s}{2\pi L r} \cos\theta_x dx \tag{4}$$

where Ps (W/m) is the flux density emitted by the 2D power source. Then the flux density absorbed by the substrate surface at time t from the center of the 2D power source is:
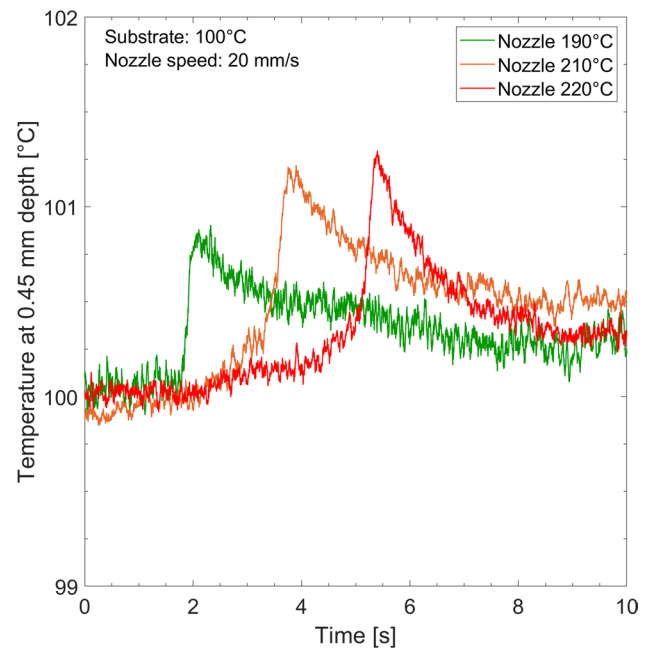
$$q = \frac{P_s d}{4\pi L} \int_{-L}^{L} \frac{1}{\left(d^2 + (vt - x)^2\right)} dx \tag{5}$$

where d is the height of the nozzle from the substrate, v the velocity of the nozzle and the time $t = l/v$.

Results and discussion

Measurements of the temperature in the substrate

Thermal measurements were performed as described in part 2.3. Figure 8 shows the influence of the nozzle passage at 20 mm/s over the substrate at 0.4 mm for three

nozzle temperatures and the substrate at 100 °C. A typical increase of temperature of about 1 °C is recorded by the thermocouples at 0.45 mm depth under the surface. The recorded curves were time shifted for better visibility. As the nozzle temperature increased, the temperature peak logically increased as radiative effects are more important. These results confirm that a vertical thermal gradient starting from surface and reaching the thermocouple at a depth of 0.45 mm is induced by the passage of the nozzle.

In Fig. 9, we investigated the influence of the regulated substrate temperature on the recorded temperature at a depth of 0.45 mm for a nozzle temperature of 210 °C. Substrate temperatures varied from 80 to 130 °C. Curves were also time shifted for better visibility. We can see how decreasing the initial temperature of the substrate increases the temperature rise detected at a depth of 0.45 mm. More generally speaking, this phenomenon will be much more important on parts printed at room temperature.

As described in Figs. 8 and 9, we were able to detect the influence of substrate and nozzle temperatures on the temperature rise at a depth of 0.45 mm under the substrate surface. Five measurements were done for each processing conditions to determine more precisely the temperature rise (Fig. 10). The standard deviation for the temperature rise calculated with 40 experiments is equal to 0.16 °C.

Based on these results, we can consider that increasing the nozzle temperature from 210 to 220 °C lead to an average elevation of 0.1 °C of the temperature peak at 0.45 mm
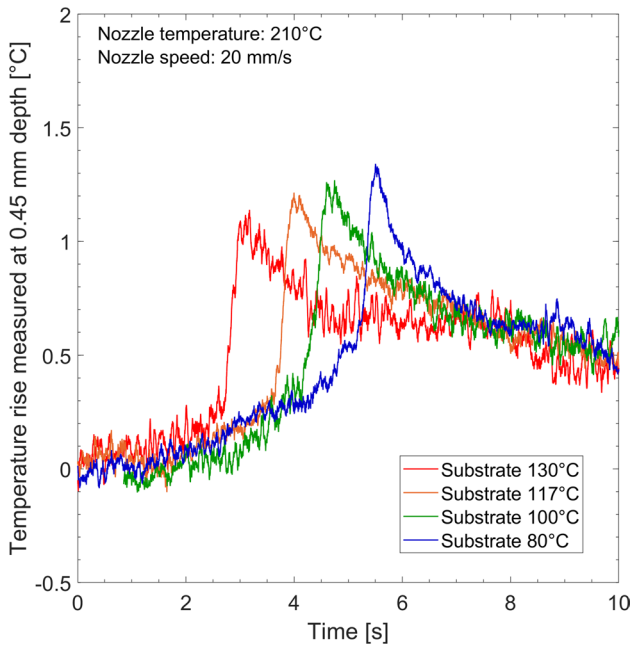
Fig. 9 Influence of substrate temperature on the temperature increase at 0.45 mm depth
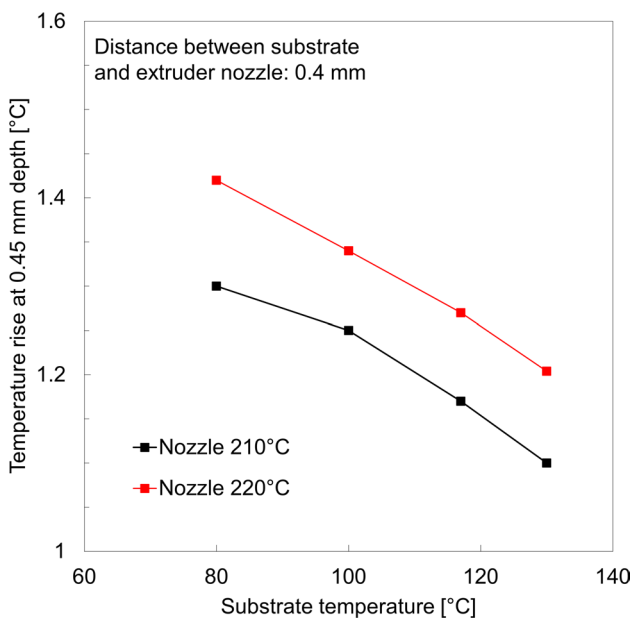
Fig. 10 Influence of nozzle and substrate temperature on the increase of temperature measured at 0.45 mm depth in the substrate

depth. The increase of the regulated substrate temperature from 90 to 130 °C induces a decrease of the temperature peak at 0.45 mm depth of about 0.2 °C.

Prediction of substrate temperature rise

In the following section, the thermal numerical model is used to predict the substrate temperature rise. Two parameters need to be adjusted to fit the experimental thermocouple measurements: the radiative flux of the nozzle Ps and the thermal contact resistance between the feedstock substrate and temperature-controlled build plate. The thermal contact resistance was set equal to 2×10^{-4} m^2 K/W. Nevertheless, this value has a low influence on the recorded temperature profile in the substrate during cooling after the nozzle passage. This is probably because the cooling is observed for a duration of 5 s while the approximated heat penetration time t_p, given by Eq. (6) to reach the interface between the substrate and the build plate from the thermocouple location is about 7 s.

$$t_p = d^2/a \qquad (6)$$

where a is the thermal diffusivity, d the travelling distance.

Therefore, the only significant fitted parameter is the radiative flux Ps (Eq. 5), which is identified to fit as much as possible the temperature peak due to the nozzle passage for all processing conditions.

Figure 11 depicts the influence of nozzle temperature on the interface temperature for a substrate temperature of 130 °C when nozzle is passing at 0.4 mm over the substrate surface. We observe a good agreement between experimental results and simulated temperatures at 0.45 mm depth with a value of nozzle radiative flux Ps of 150 and 170 W/m for a nozzle temperature of respectively 210 °C and 220 °C. While the measured temperature at 0.45 mm from the substrate surface increases by about 1 °C, the temperature at substrate surface increases by about 3.5 °C for these conditions. More precisely, an increase of nozzle temperature from 210 to 220 °C increases the temperature at the surface of the substrate from 3.2 to 3.6 °C. A shift of about 0.3 s can be noted between the temperature peak at the substrate surface and the one measured at a depth of 0.45 mm under the substrate surface, which is also consistent with the order of magnitude of heat penetration time (Eq. 6).

According to Eq. 5, the absorbed radiative flux by the substrate is directly proportional to radiative flux Ps emitted by the nozzle. We ensured that the simulated increase of temperature (peak height) is also proportional to the value of Ps. Therefore, the values of Ps (Fig. 12), which fit the whole experimental data can be directly deduced from the measured values of temperature rises in Fig. 10.

The variation of Ps values (between 155 and 200 W/m) depending on nozzle and substrate temperatures for a nozzle passage at 0.4 mm from the substrate are consistent with the Stefan-Boltzmann law: the emitted radiative flux and the absorbed radiative flux only depend on the temperatures of
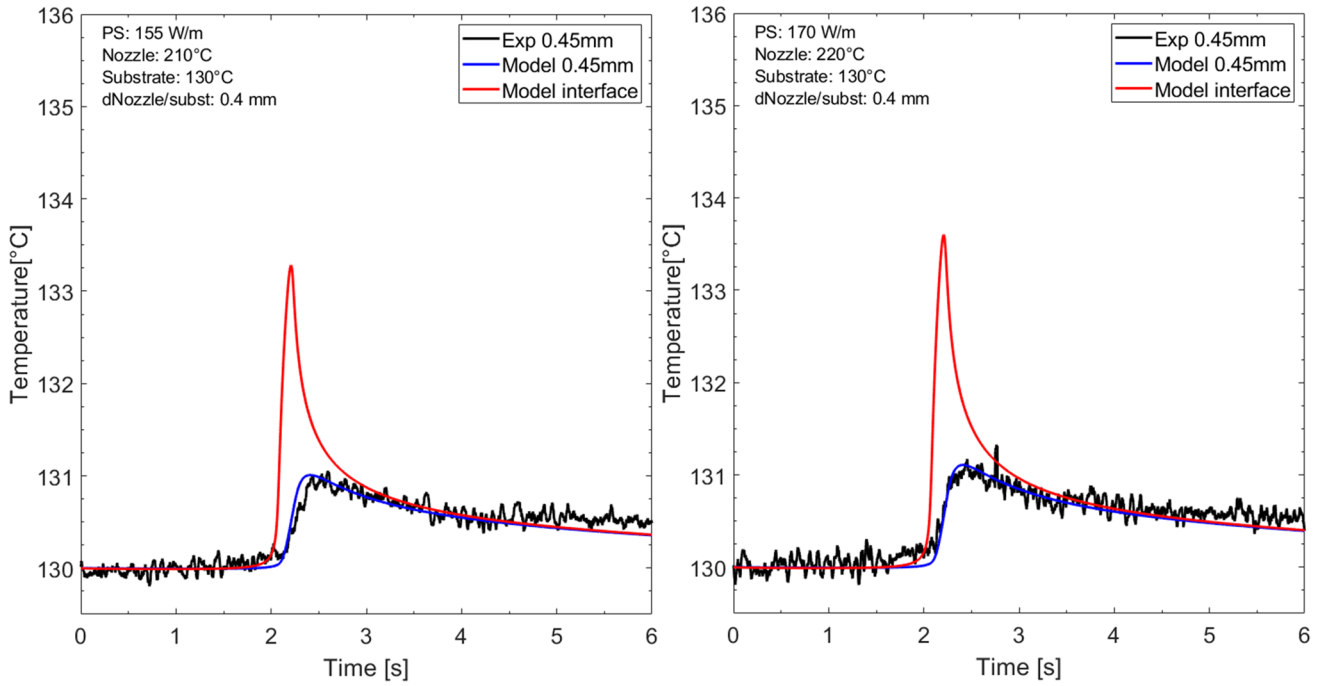
Fig. 11 Influence of nozzle temperature on predicted temperature rise at substrate surface for a substrate at regulated at 130 °C and a substrate-nozzle distance equal to 0.4 mm. Left—nozzle at 210 °C, right—nozzle at 220 °C
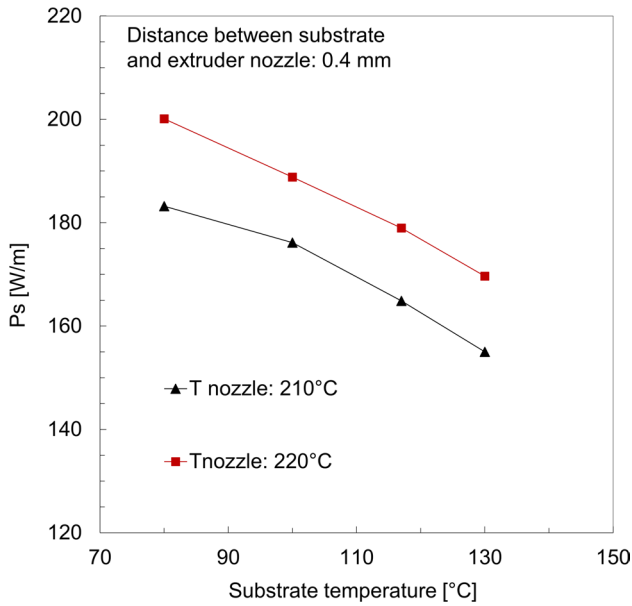

Fig. 12 Simulated absorbed radiative flux to fit experimental data for a nozzle passage at 0.4 mm from the substrate
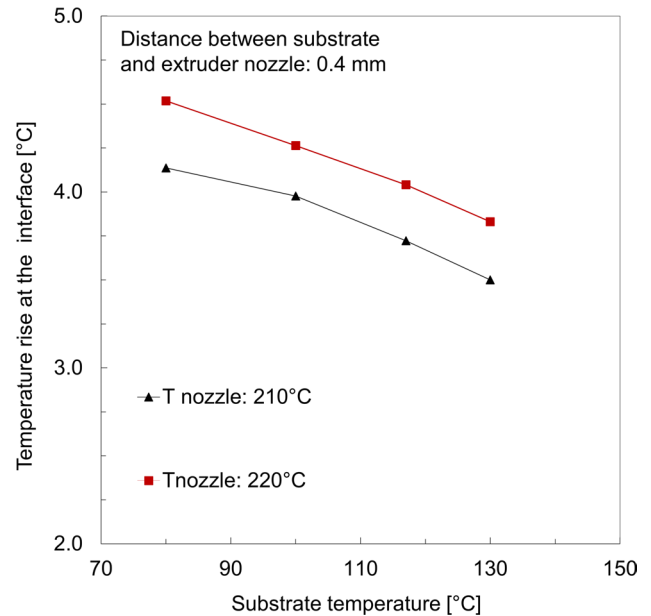
Fig. 13 Simulated temperature rise of the substrate surface for a nozzle passage at 0.4 mm from the substrate

the source and the absorbent surface, with the radiative flux depending of the temperature at the power 4.

At least, if we consider a nozzle width of 3 mm, a mean absorbed radiative flux by the nozzle would be about 0.5 W.

The simulated rises of temperature at the substrate surface for the different nozzle and substrate temperatures and for a nozzle passage at 0.4 mm from the substrate surface are reported in Fig. 13.

In that FFF process, a layer of 0.2 mm is often performed on parts. Then, measurements and simulations were performed for a nozzle passage at a distance of 0.2 mm of the substrate temperature. Figure 14 shows a comparison between numerical and experimental results. But Ps values of 200 W/m and 220 W/m were needed instead of 175 W/m and 190 W/m (Fig. 11) to correctly fit the experimental data for respectively nozzle temperatures at 210 and 220 °C and a substrate temperature at 100 °C.

It means that the substrate surface is still more heated than the one predicted by the modelling (Eq. 5) and that the radiative heating is probably not the only physical phenomenon to take into account. At this exceedingly small distance of 0.2 mm, air convection effects should perhaps not be neglected and may also play a role in the heating of the substrate surface. We also considered that all the emitted radiation is absorbed, but the reflection on the substrate may be lower when the nozzle is passing at 0.2 mm than
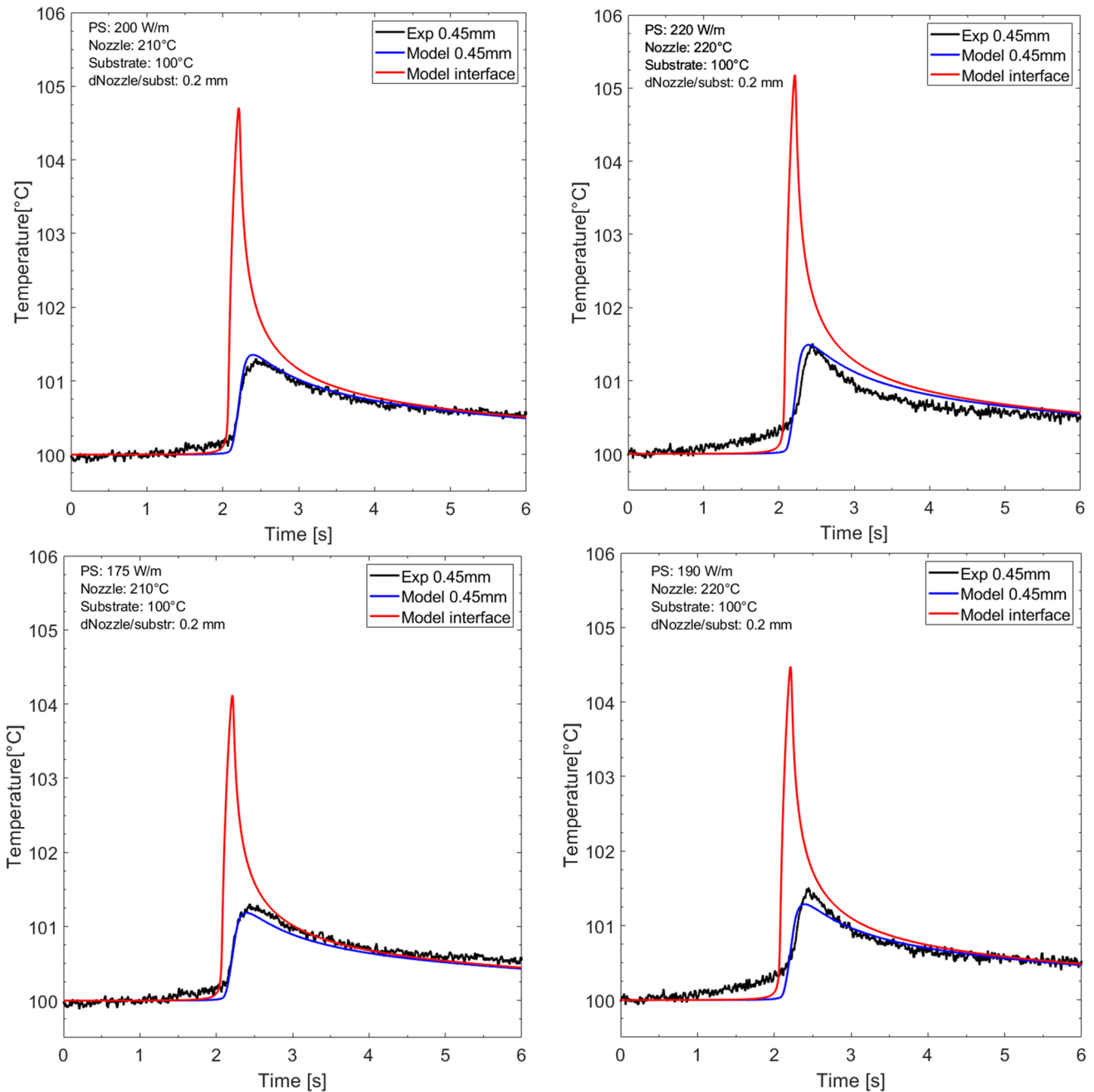
Fig. 14 Influence of emitted radiative flux density Ps on predicted temperature for the substrate heated at 100 °C and for a substrate-nozzle distance equal to 0.2 mm. Left—nozzle at 210 °C, right—nozzle at 220 °C

at 0.4 mm. These two phenomena could explain the small gap between simulations and experiments.

Moreover an increase in temperature appears before the peak and is not described by the model. It is due to the geometry of the nozzle, which was extremely simplified in the thermal modelling. Nevertheless, we managed to fit quite well the sudden increase of temperature. We tried to refine the nozzle geometry by adding another emitted radiative flux at a higher distance of the substrate and we managed to improve the experimental fit before the peak. We did not integrate this refinement because we were still far from the real geometry of the nozzle and we wanted to focus on the most important interface temperature variation: the peak.

Conclusion

In FFF process, the hot nozzle moves a few tenths of a millimeter above the substrate or deposited filaments. This study quantifies the thermal effect of the radiation emitted by the nozzle on the surface temperature of a feedstock material, which plays a key role on the adhesion between layers.

To avoid disturbing the temperature field at the surface of the feedstock substrate by an intrusive measuring element, 0.25 mm diameter thermocouples were inserted in 0.3 mm diameter holes at 0.45 mm under the substrate surface. This methodology was proven to be precise and fairly easy to implement. A temperature rise varying between 1.1 and 1.5 °C was measured while the extrusion nozzle was passing above the substrate surface for different processing conditions.

To determine the rise of temperature at the substrate surface, a simple 2D thermal model using finite-difference method with an explicit scheme was built on Matlab® code. The nozzle was modelled as simple 2D plate moving over the substrate and emitting a fixed radiative flux, which was fully absorbed by the substrate and which was identified to fit as much as possible the temperature measurements recorded by the thermocouples.

A particularly good temperature evolution was found for all processing conditions between simulated and recorded temperatures, which gives confidence in predicted temperatures at the surface of the substrate: a temperature rise between 3.5 and 5 °C. Increasing the nozzle temperature, decreasing the controlled substrate temperature or decreasing the distance between nozzle and substrate logically increases the temperature rise at the surface, which is favorable to filament adhesion. For the processing conditions of the studied feedstock material, the absorbed radiative flux of the nozzle was assessed to be about 0.5 W, a value that can vary by 20% depending on process conditions.

Therefore, we shown that a thermal simulation of the FFF process must consider this radiative effect of the nozzle to precisely determine the temperature evolution of the substrate surface, a data necessary for the prediction of good adhesion properties between the layers.

Declarations

Conflict of interest All the authors declare that they have no conflict of interest.

References

1. German RM (2019) Metal powder injection molding (MIM): key trends and markets. In: Heaney FD (ed) Handbook of metal injection molding, 2nd edn. Woodhead Publishing, Cambridge, pp 1–25
2. Gonzalez-Gutierrez J, Cano S, Schuschnigg S et al (2018) Additive manufacturing of metallic and ceramic components by the material extrusion of highly-filled polymers: a review and future perspectives. Materials 11:840
3. Rane K, Strano M (2019) A comprehensive review of extrusion-based additive manufacturing processes for rapid production of metallic and ceramic parts. Adv Manuf 7:155–173. https://doi.org/10.1007/s40436-019-00253-6
4. Regnier G, Le Corre S (2016) Modeling of thermoplastic welding. Heat transfer in polymer composite materials. Wiley ISTE Ltd, Hoboken, pp 235–268
5. Wool RP, O'Connor KM (1981) A theory of crack healing in polymers. J Appl Phys 52:5953–5963. https://doi.org/10.1063/1.328526
6. de Gennes PG (1971) Reptation of a polymer chain in the presence of fixed obstacles. J Chem Phys 55:572–579. https://doi.org/10.1063/1.1675789
7. Doi M, Edwards SF (1978) Dynamics of concentrated polymer systems. Part 1.—Brownian motion in the equilibrium state. J Chem Soc 74:1789–1801
8. Yang F, Pitchumani R (2002) Healing of thermoplastic polymers at an interface under nonisothermal conditions. Macromolecules 35:3213–3224. https://doi.org/10.1021/ma010858o
9. Partain SC (2007) fused deposition modeling with localized pre-deposition heating using forced air. Master thesis, Montana State University
10. Striemann P, Hülsbusch D, Niedermeier M, Walther F (2020) Optimization and quality evaluation of the interlayer bonding performance of additively manufactured polymer structures. Polymers 12:1166. https://doi.org/10.3390/polym12051166
11. Ravi AK, Deshpande A, Hsu KH (2016) An in-process laser localized pre-deposition heating approach to inter-layer bond strengthening in extrusion based polymer additive manufacturing. J Manuf Process 24:179–185. https://doi.org/10.1016/j.jmapro.2016.08.007
12. Deshpande A, Ravi A, Kusel S et al (2019) Interlayer thermal history modification for interface strength in fused filament

fabricated parts. Prog Addit Manuf 4:63–70. https://doi.org/10.1007/s40964-018-0063-1

13. Seppala JE, Migler KD (2016) Infrared thermography of welding zones produced by polymer extrusion additive manufacturing. Addit Manuf 12:71–76. https://doi.org/10.1016/j.addma.2016.06.007

14. Lepoivre A, Boyard N, Levy A, Sobotka V (2020) Heat transfer and adhesion study for the FFF additive manufacturing process. In: Bambach M (ed) Procedia manufacturing. Elsevier, Amsterdam, pp 948–955

15. Xu D, Zhang Y, Pigeonneau F (2021) Thermal analysis of the fused filament fabrication printing process: experimental and numerical investigations. Int J Mater Form 14:763–776. https://doi.org/10.1007/s12289-020-01591-8

16. Wolszczak P, Lygas K, Paszko M, Wach RA (2018) Heat distribution in material during fused deposition modelling. Rapid Prototyp J 24:615–622. https://doi.org/10.1108/RPJ-04-2017-0062

17. Cosson B, Asséko ACA (2019) Effect of the nozzle radiation on the fused filament fabrication process: three-dimensional numerical simulations and experimental investigation. J Heat Transfer 141:082102. https://doi.org/10.1115/1.4043674

18. Bedoui F, Fayolle B (2014) POM mechanical properties. In: Lüftl S, Visakh PM, Chandran S (eds) Handbook od polyoxymethylene. Wiley, Hoboken, pp 241–255. https://doi.org/10.1002/9781118914458.ch9

19. Kowalski L, Duszczyk J, Katgerman L (1999) Thermal conductivity of metal powder-polymer feedstock for powder injection moulding. J Mater Sci 34:1–5. https://doi.org/10.1023/A:1004424401427

20. Pearce JV, Montag V, Lowe D, Dong W (2011) Melting temperature of high-temperature fixed points for thermocouple calibrations. Int J Thermophys 32:463–470. https://doi.org/10.1007/s10765-010-0892-8

21. Rodriguez JF, Thomas JP, Renaud JE (2000) Characterization of the mesostructure of fused-deposition acrylonitrile-butadiene-styrene materials. Rapid Prototyp J 6:175–186. https://doi.org/10.1108/13552540010337056

22. Bellehumeur C, Li L, Sun Q, Gu P (2004) Modeling of bond formation between polymer filaments in the fused deposition modeling process. J Manuf Process 6:170–178. https://doi.org/10.1016/S1526-6125(04)70071-7

23. Delaunay D, Le Bot P, Fulchiron R et al (2000) Nature of contact between polymer and mold in injection molding. Part I: influence of a non-perfect thermal contact. Polym Eng Sci 40:1682–1691. https://doi.org/10.1002/pen.11300